# Velocity redistribution of excited atoms by radiative excitation transfer. I. Experimental demonstration by photodissociation of $Na_2$ and field-free imaging

O. Kaufmann, A. Ekers,[a] and K. Bergmann
*Department of Physics, University of Kaiserslautern, Erwin-Schrödinger-Str., D-67663 Kaiserslautern, Germany*

N. Bezuglov
*Fock Institute of Physics, St. Petersburg State University, Petrodvorets, Ulianovskaya ul. 1, 198904 St. Petersburg, Russia*

K. Miculis and M. Auzinsh
*Institute of Atomic Physics and Spectroscopy, University of Latvia, Raiņa bulv. 19, LV-1586 Riga, Latvia*

W. Meyer
*Department of Chemistry, University of Kaiserslautern, Erwin-Schrödinger-Str., D-67663 Kaiserslautern, Germany*

(Received 21 March 2003; accepted 13 May 2003)

Photodissociation of state-selected sodium molecules, $Na_2(X\,^1\Sigma_g^+, v'') + h\nu \rightarrow Na_2^*(B\,^1\Pi_u) \rightarrow Na^*(3p_{3/2}) + Na(3s_{1/2})$ has been studied theoretically and experimentally using a novel ''field-free'' ion imaging design. The experiment uses a supersonic $Na/Na_2$ beam in combination with the stimulated Raman adiabatic passage technique to prepare $Na_2$ molecules in selected rovibronic levels of the electronic ground state. The $Na(3p_{3/2})$ fragments are photoionized (or excited to high Rydberg states) in a permanently field-free reaction zone. The fragments enter the ion optics because of the flow velocity of the beam and are focused onto a position sensitive detector, which provides an energy resolution of about 50 meV. The measured anisotropic photofragment angular distributions reflect the alignment of the molecules prior to dissociation and are well explained by the anisotropic nature of the photodissociation by polarized laser light. The measured images show not only the expected relatively fast photodissociation fragments, but also the efficient formation of slow $Na(3p_{3/2})$ atoms. Fast and slow refer to the atomic velocity relative to the center of-mass of the dissociating molecule. The ratio of the numbers of slow atoms and fast photofragments is 0.16 and 0.22 for the dissociation of $Na_2$ from levels $v''=17$ and $v''=23$, respectively. Several models are analyzed to explain the observations. Calculations show that the dramatic velocity redistribution is caused by radiation trapping: the excitation is efficiently radiatively transferred from the fast $Na(3p)$ photofragments to the abundant $Na(3s)$ atoms from the primary beam, whereby the hyperfine splitting of the $3s$ state must be taken into account. Analytical formulas describing this mechanism show a ratio of slow to fast $Na(3p)$ atoms of 0.13 for $v''=17$ and 0.19 for $v''=23$, which is in very good agreement with the experimental observations.
 [DOI: 10.1063/1.1589474]

## I. INTRODUCTION

The velocity and angular distributions of molecular reaction fragments carry important information about the molecular dynamics. The determination of these distributions is therefore essential in studies of chemical reaction dynamics,[1,2] photofragmentation,[3] or dissociative electron attachment.[4] Some 15 years ago, Chandler and Houston[5] proposed and demonstrated the powerful ion imaging method. By measuring the two-dimensional projection of the three-dimensional spatial fragment distribution simultaneous detection of fragment velocity, angular, and internal energy distributions is achieved. Ion imaging methods have become commonly used techniques for the study of uni- and bimolecular fragmentation processes (see the reviews[6–10]).

Ion imaging apparatus usually use electric fields to extract the ionized fragments from the reaction region. However, when atoms or molecules in Rydberg states are involved, the extraction field will ionize them.[11] The resulting high density of electrons and ions may blur the processes to be studied.[12,13] We have therefore developed an ion imaging apparatus with a permanently field-free reaction zone.[14] We have applied this field-free apparatus to study the photofragmentation of $Na_2$ via the $B\,^1\Pi_u$ state (see Fig. 1):

$$Na_2(X\,^1\Sigma_g^+, v'') + h\nu \rightarrow Na_2^*(B\,^1\Pi_u) \rightarrow Na(3p_{3/2}) + Na(3s_{1/2}) + \Delta E_{diss}(v''). \quad (1)$$

[a]Author to whom correspondence should be addressed. Electronic mail: ekers@physik.uni-kl.de

 

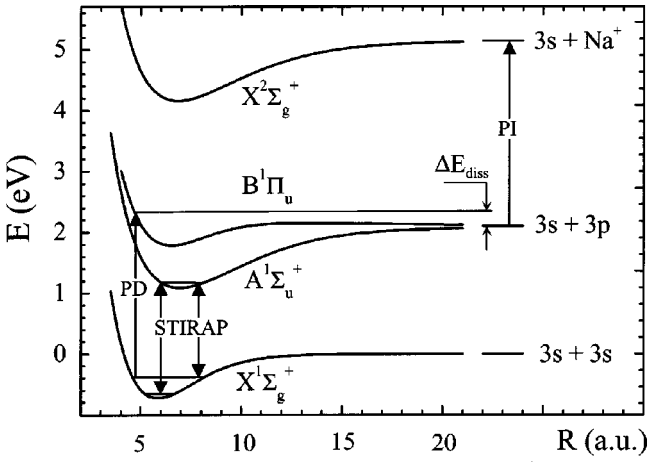


FIG. 1. An illustration of the photodissociation scheme used in the present experiment. The $Na_2$ molecules are selectively prepared in excited rovibronic levels of the electronic ground state $X\,^1\Sigma_g^+$ by means of STIRAP via the $A\,^1\Sigma_u^+$ state. The molecules are photodissociated from these excited rovibronic levels by the $\lambda_{PD}=458$ nm photons from an $Ar^+$ ion laser via the $B\,^1\Pi_u$ state. The excess energy $\Delta E_{diss}$ is transformed in equal amounts into the translation energies of the Na*$(3p_{3/2})$ and Na$(3s)$ fragments. The excited Na*$(3p_{3/2})$ photofragments are photoionized or excited to high Rydberg states ($\lambda_{PI}\approx 408$ nm) and registered by an ion imaging detector.

As a two-body fragmentation with a single dissociation channel, this process is suitable for assessing the properties of the field-free imaging setup. The molecules are selectively prepared in single rovibronic levels using the stimulated Raman adiabatic passage (STIRAP) technique.[15] The well-defined initial quantum state in combination with the control of laser polarizations allows the production of photofagments with well-defined kinetic energies and angular distributions. As the potential energy curves of the $Na_2$ molecule are well known, it is straightforward to describe this fragmentation process theoretically for comparison with the experimental two-dimensional photofragment images. Surprisingly, the experiments reveal that this seemingly simple photofragmentation process is accompanied by an efficient secondary process that produces low-energy Na$(3p_{3/2})$ atoms. As will be shown below, this observation is caused by efficient radiative excitation transfer from the Na$(3p_{3/2})$ photofragments to the Na$(3s)$ atoms in the primary beam. In Secs. II and III we shall describe the experiment and give the results. Section IV is devoted to the theoretical description of the photodissociation process (1). Section V explains the dramatic velocity redistribution of excited atoms by radiation trapping. A full derivation of this theory is given in the accompanying publication.[16]

## II. EXPERIMENTAL SET-UP

### A. Supersonic beam

For the experiments we use a single supersonic beam of sodium atoms and molecules (see Fig. 2). The vacuum apparatus consists of four differentially pumped chambers containing the source oven, the section for the optical preparation of molecules, the reaction region with ion optics, and the imaging detector. The expansion of sodium vapor from the source at 900 K temperature through a 0.4 mm diam nozzle yields vibrationally and rotationally cold molecules with 99% of the population in the ground vibrational level $v''=0$. The maximum of the distribution over rotational levels is at $J''=7$. The flow velocity is $v_f=1340$ m/s, and the $1/e$ widths of the longitudinal velocity distributions are $\Delta v_{at}=300$ m/s and $\Delta v_{mol}=260$ m/s for the atoms and molecules, respectively. The beam is collimated by two skimmers and a 2 mm diam aperture at the entrance of the reaction zone. The resulting divergence of 0.8° leads to a residual transverse Doppler width of 30 MHz. The densities of atoms and molecules in the reaction region 20 cm downstream from the nozzle are $2\times10^{11}$ and $2\times10^{10}$ $cm^{-3}$, respectively.

### B. Optical preparation and fragmentation of the molecules

The relevant optical transitions are shown in Fig. 1. The molecules are selectively prepared in excited $(v_f'',J_f'')$ rovibronic levels in the electronic ground state by means of the STIRAP technique.[15] The Stokes laser field (Coherent CR-899 Ti:Sa, 1 MHz linewidth, a few hundred mW power) couples an intermediate $(v',10)$ level in the $A\,^1\Sigma_u^+$ state with

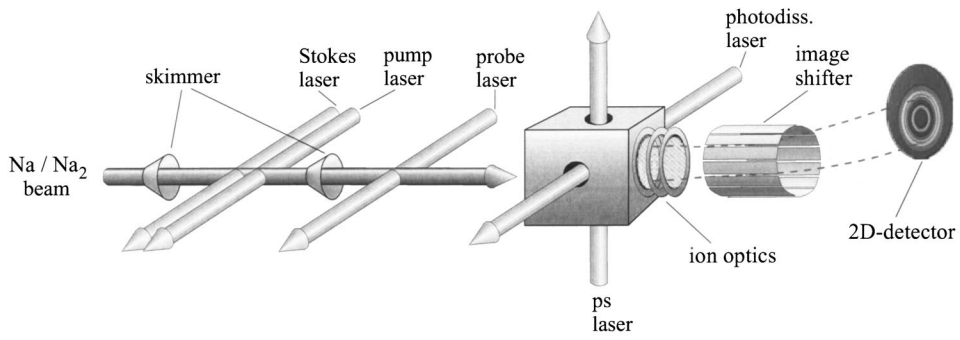


FIG. 2. An arrangement of the experiment with field-free ion imaging. The partially overlapping Stokes and pump lasers serve for the selective vibrational excitation of the molecules by means of STIRAP. The probe laser allows monitoring of the vibrational excitation, and it is shut off during the detection of fragments by ion imaging. The photodissociation laser fragments the $Na_2$ molecules into Na$(3p)$ and Na$(3s)$ atoms inside the electrostatically screened reaction chamber. The frequency doubled radiation from a picosecond (ps) laser ionizes the Na$(3p)$ fragments or excites them to high Rydberg states. The ions leave the field-free zone through a fine mesh at expense of their translation energy and enter the ion optics. The ion optics is operated in the velocity mapping mode and focuses the ions onto a two-dimensional position sensitive detector (PSD). The PSD is displaced from the molecular beam axis to prevent neutral atoms and molecules of the primary beam from reaching its surface. The ions are correspondingly deflected away from the beam axis toward the detector by a homogeneous field of the electrostatic image shifter.

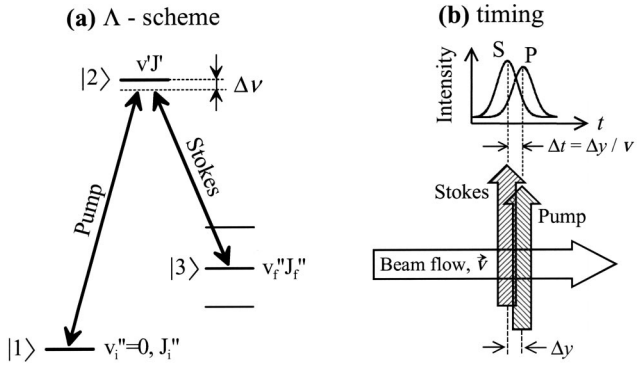


FIG. 3. (a) The coupling scheme for STIRAP. The Stokes laser field couples the intermediate $v'J'$ level with the desired final $v_f''J_f''$ level before the interaction with the pump laser field takes place. Both laser frequencies are detuned by an equal amount $\Delta\nu$ from resonance with the molecular transitions, maintaining two-photon resonance. (b) The Stokes laser beam axis is shifted upstream from the pump laser beam. The molecules traveling in the particle beam with flow velocity $v_f$ are thus exposed to the Stokes laser field prior to the pump laser field.

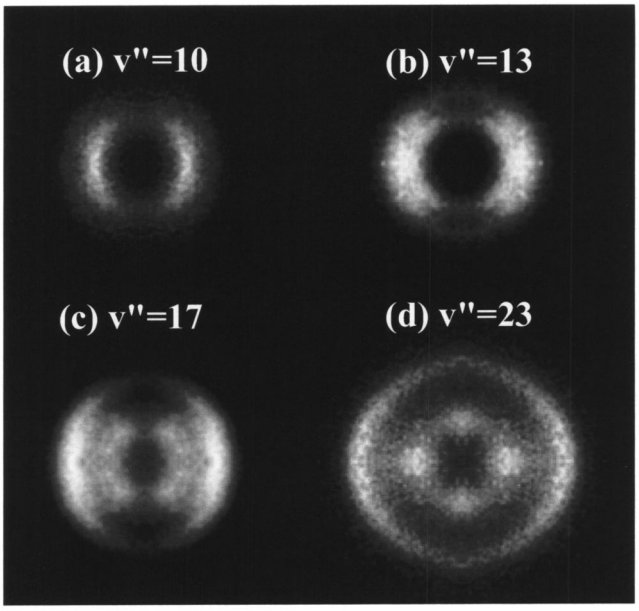


FIG. 4. Experimental 2-D images of photoionized Na($3p_{3/2}$) fragments resulting from the photodissociation of $Na_2$ molecules selectively excited to robrivonic levels $v''$, $J''=9$ in the electronic ground state: (a) $v''=10$; (b) $v''=13$; (c) $v''=17$; (d) $v''=23$. In order to increase the signal-to-noise ratio for reconstruction purposes, the images are two-fold symmetrized and smoothed using a 2-D Gaussian filter, averaging over five points.

the desired final $(v_f'',9)$ level in the $X\,^1\Sigma_g^+$ state before a pump laser field (Coherent CR-699, DCM dye, 1 MHz linewidth, a few hundred mW power) couples the initial (0, 9) with the intermediate level [Fig. 3(a)]. Both laser beams cross the particle beam at right angles and are polarized perpendicularly to the particle beam axis. They are focused by a cylindrical lens with the focus placed at the particle beam axis in the optical preparation chamber. The proper sequence of laser pulses is achieved by shifting the Stokes laser axis slightly upstream from the pump laser beam [see Fig. 3(b)]. Both laser frequencies are detuned off resonance by an equal amount of $\Delta\nu=200$ MHz. The above scheme ensures a population transfer efficiency of up to 99%, as monitored by probing the population in the desired final level by laser-induced fluorescence on the $A\,^1\Sigma_u^+(v'_{pr},10)\leftarrow X\,^1\Sigma_g^+(v_f'',9)$ transitions downstream from the optical preparation chamber. The optical preparation of the molecules is spatially separated from the reaction region (see Fig. 2) to avoid that any processes induced by the laser light used for vibrational excitation interfere with the photodissociation process.

The molecules in levels $v''\geqslant 10$ are photodissociated into Na($3p_{3/2}$) and Na($3s_{1/2}$) fragments by the $\lambda_{PD}=458$ nm radiation from an $Ar^+$ ion laser via the $B\,^1\Pi_u$ state. The $Ar^+$ laser beam with a power of typically 250 mW crosses the particle beam axis at right angles in the reaction chamber. It is polarized perpendicularly to the particle beam axis and focused to a spot of *ca.* 2 mm diam. The Na($3p_{3/2}$) fragments are photoionized (or excited to high Rydberg states—see Sec. III) by the frequency doubled radiation ($\lambda_{PI}$ tunable around 408 nm) of a mode locked Ti:Sa laser (Coherent MIRA-900-P, 3 ps pulse length, 76 MHz repetition rate), and detected by an ion imaging detector.

### C. "Field-free" ion imaging detector

A detailed description of the ''field-free'' imaging apparatus is given in Ref. 14. Briefly, a permanently field-free reaction zone is an essential feature of our imaging setup. After fragmentation and possibly ionization, the particles propagate freely to the mesh that separates the field-free zone and the ion optics region. Their location at the entrance depends on the momentum perpendicular to the particle beam axis acquired in the fragmentation process. The ion optics consists of two cylindrical electrodes placed on the particle beam axis downstream from the reaction chamber. The ion optics accelerates and images the charged fragments onto a position sensitive detector (PSD), consisting of multichannel plates (MCPs) in the Chevron arrangement followed by a phosphor screen and a charge coupled device (CCD) camera (La Vision, 640×480 pixels). The two-dimensional (2-D) photofragment images registered by the PSD are stored and processed using the La Vision DaVis 5.4.4 software. The PSD is displaced from the particle beam axis to prevent the sodium atoms and molecules of the primary beam from hitting (and thus destroying) the MCPs. The ionic fragments are deflected away from the particle beam axis onto the PSD by a homogeneous electrostatic field of the dodecapole image shifter.[17,18] The exit plane of the ion optics is screened from the deflection field by a fine mesh. The voltages applied to the electrodes of ion optics can be varied to switch between the space-mapping[5] and velocity-mapping[19] modes. The latter was preferred since it provides a significantly better resolution of the images.

## III. RESULTS

Figure 4 shows the photofragment 2-D images resulting from the dissociation of $Na_2$ from levels $v''=10$, 13, 17, and 23 in the ground electronic state. They correspond to the fragment kinetic energies of 27, 54, 87, and 136 meV, respectively. We did not observe any fragmentation from the level $v''=9$, which shows that tunneling from this level is

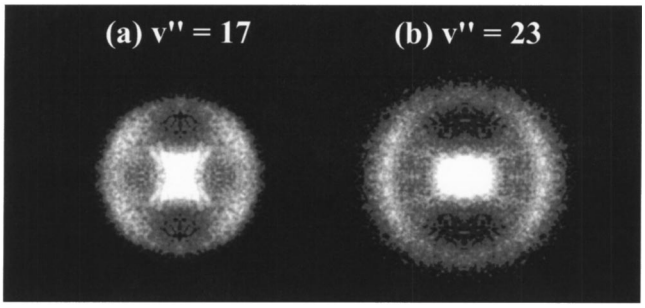


FIG. 5. Experimental 2-D images of Na($3p_{3/2}$) fragments excited to high Rydberg states. They result from the photodissociation of $Na_2$ molecules selectively excited to rovibronic levels $v''$, $J''=9$ in the electronic ground state: (a) $v''=17$; (b) $v''=23$. The images are two-fold symmetrized and smoothed using a 2-D Gaussian filter.

negligible. The outer ring on each figure is the image of photoionized fragments resulting from the photodissociation of the molecule. As expected, the radius of the ring increases proportionally to $v=\sqrt{2E/m}$. However, the presence of the inner ring clearly seen on images for $v''=17$ and 23 and hardly resolvable for $v''=13$ is surprising. It is observed only when the molecules are vibrationally excited and the radiation of both the photodissociation laser and the photoionization laser is present. In addition, the radius of this inner structure does not change with the vibrational level $v''$. (For $v''=10$ the inner ring overlaps with the ring of the photofragment image.) This observation suggests that the inner structure of the images does not result from a direct photodissociation of $Na_2$.

The following observation leads us to the conclusion that the particles observed near the center of the image are not the fragments of photodissociation. We tuned the energy of the photoionizing photons to just below the Na($3p_{3/2}$)$\rightarrow Na^+$ ionization threshold and excited the Na($3p_{3/2}$) fragments to high Rydberg states. The particles should still be properly imaged since they are ionized by the electrostatic fields of the ion optics immediately after entering it. These images are shown in Fig. 5. As expected, the photofragment images have remained unchanged compared to Fig. 4, while the inner ring has contracted to a spot in the middle of the image corresponding to zero velocity perpendicular to the primary beam axis. Such a transformation of the inner structure when the frequency of the ionizing laser is tuned below the Na($3p_{3/2}$)$\rightarrow Na^+$ ionization threshold allows us to relate this structure to Na($3p_{3/2}$) atoms. In Sec. V we shall show that they result from a dramatic radiative population redistribution between the excited Na($3p_{3/2}$) photofragments and the abundant Na($3s_{1/2}$) atoms from the sodium beam. The ratio of the number of particles in the middle spot corresponding to ''slow'' Na($3p_{3/2}$) atoms to the number of faster photofragments in the outer ring is about 0.4. This value is approximately the same for the dissociation from levels $v''=17$ and $v''=23$ as determined from the images in Fig. 4 and in Fig. 5. The determination of the ratio from images of photodissociation from levels $v''=10$ and $v''=13$ is ambiguous since the inner and outer structures are not resolved. However, the determination of the ratio of slow-to-fast excited atoms from the raw images on Fig. 5 is not exactly correct. It is because the fast photofragments are distributed within the entire area of the 2-D detector limited by the intense outer ring. Therefore the intensity of the central spot of the image includes also a nonzero contribution of the fast photofragments. Therefore the value of 0.4 is to be considered as the upper limit of the ratio. In order to correctly determine the ratio, the contributions of the fast and the slow excited atoms should be separated. As will be shown at the end of Sec. IV B, such separation is possible by reconstructing the original 3-D distribution of the excited atoms by means of the inverse Abel transformation. Such separation yields for the ratio of numbers of slow and fast excited atoms a value of 0.16 for $v''=17$ and 0.22 for $v''=23$.

The sensitivity of the ''slow'' Na($3p_{3/2}$) atoms to the ionization threshold can be explained by the properties of the field-free imaging design (see Ref. 14 for a detailed description). Any stray electric fields in the permanently field-free zone of the reaction chamber affect the trajectories of charged particles and thus change the images beyond the ion optics. Electric stray fields may arise from, e.g., any rest or patch surface potentials, or the presence of ions in the particle beam. Furthermore, the exposure of mesh separating the field-free reaction zone from the ion optics to the particle beam leads to deposition of sodium onto the mesh. This exposure leads to a build-up of a contact potential between the stainless steel mesh and the deposited sodium. The image quality becomes noticeably distorted after only 5 min of operation. The detrimental consequences of space charges were observed in a separate experiment in which $Na^+$ ions were created by means of two-step ($3s\rightarrow 3p\rightarrow$continuum) photoionization of Na($3s_{1/2}$) atoms from the primary beam.[14] Already at moderate intensities of the laser exciting the $3s\rightarrow 3p$ transition (well below saturation) the ion density was high enough to cause dramatic Coulomb repulsion between the photoions. In contrast, excitation of the Na($3p$) atoms to high Rydberg states showed no such repulsion at a weak excitation of the $3s\rightarrow 3p$ transition. In fact, the Coulomb repulsion is important for the ions traveling parallel to the beam axis, while the ionized photofragments leave the beam quickly and their trajectories are less sensitive to space charge near the particle beam axis. Therefore we consider the images taken with particles excited to high Rydberg states as properly reflecting their velocity distribution.

The photofragment images, Figs. 4 and 5, clearly show an anisotropy in the photofragment angular distribution. The calculations presented below in Sec. IV suggest that the distribution should be close to $\sin^2\theta$, where $\theta$ is the angle between the polarization vector of the dissociating laser and the velocity direction of the photofragments. The laser polarization direction defines the symmetry axis of the 3-D photofragment distribution and, consequently, the symmetry axis of its 2-D projection (the vertical axis in Figs. 4 and 5; see also Fig. 7 for reference). In order to correctly determine the photofragment angular distribution, the original 3-D photofragment distribution should be restored. This is done in Sec. IV B, where a comparison with the theory is provided. From the width of the measured 2-D images we find the energy resolution of the field-free imaging detector to be, on average, 50 meV.

## IV. ANALYSIS: PHOTODISSOCIATION

The photodissociation process under study is illustrated in Fig. 1. The $B\,^1\Pi_u$ state correlates with the $3p_{3/2}+3s_{1/2}$ states of separated atoms and exhibits a 46 meV high potential barrier above the dissociation asymptote.[20] The absorption of one 458 nm photon from the $Ar^+$ laser provides enough energy for molecules from levels $v''\geqslant 10$ to pass over the barrier and separate into $Na(3p_{3/2})$ and $Na(3p_{1/2})$ atoms. The known experimental studies of this process have all been performed without a well-defined initial rovibronic level of $Na_2$ and with no or only indirect angular or energy resolution of photofragments.[21–24] A theoretical study[25] predicted that the $3p_{1/2}+3s_{1/2}$ asymptote can also be populated due to nonadiabatic coupling at large internuclear distances. Although in the vapor cell experiment[21] a relatively small population in the $3p_{1/2}$ level was observed, experiments using molecular beams[22–24] failed to detect any fluorescence from the $3p_{1/2}$ level at photodissociation by the 458 nm laser photons. It is therefore justified to assume that only the $j=3/2$ component of the $3p$ state is populated in this dissociation.

### A. Photodissociation cross sections

Since the potential curves of $Na_2$ are well known,[26] the theoretical modeling of the photodissociation process is straightforward. Standard methods can be used to calculate the photodissociation cross sections. The molecules are excited from a rovibronic level with energy $E(v''J'')$ in the electronic ground state into a dissociation continuum of the $B\,^1\Pi_u$ state with energy $\varepsilon=E(v''J'')+h\nu_{Ar^+}$. In the Born–Oppenheimer approximation, the initial and final molecular eigenstates factorize into electronic and nuclear parts:

$$|X\,^1\Sigma_g^+,v''J''M''\rangle=|X\,^1\Sigma_g^+\rangle_{\rm el}|v''J''M''\rangle_{\rm nuc};$$

$$|B\,^1\Pi_u,\varepsilon J'M'\rangle=|B\,^1\Pi_u\rangle_{\rm el}|\varepsilon J'M'\rangle_{\rm nuc},$$

where $M$ is the projection of the nuclear angular momentum $J$ onto the laboratory $z$ axis. The cross section of the photofragmentation depends on the photon energy and the square of the transition moment.[27,28] For linearly polarized light and isotropic distribution of the molecular axis it can be written as

$$\sigma(X\,^1\Sigma_g^+,v''J''\rightarrow B\,^1\Pi_u,\varepsilon J')=\frac{8\pi}{3c}\frac{\nu}{2J''+1}\sum_{J'=J''-1}^{J''+1}R^2_{X\,^1\Sigma_g^+,v''J''\rightarrow B\,^1\Pi_u,\varepsilon J'}\times\xi_{X\,^1\Sigma_g^+,J''\rightarrow B\,^1\Pi_u,J'}.$$

Here, $c$ is the speed of light, $\xi_{X\,^1\Sigma_g^+,J''\rightarrow B\,^1\Pi_u,J'}$ is the sum of squares of the angular part of the transition moment over the magnetic quantum number $M$ with $\Delta M=0$,[29,30]

$$\xi_{X\,^1\Sigma_g^+,J''\rightarrow B\,^1\Pi_u,J'}=\sum_{M=-J}^{+J}|R^{\rm rot}_{J''J'}|^2=\frac{1}{3}(2J''+1)(2J'+1)\begin{pmatrix}J'' & 1 & J'\\ 0 & 1 & -1\end{pmatrix}^2$$

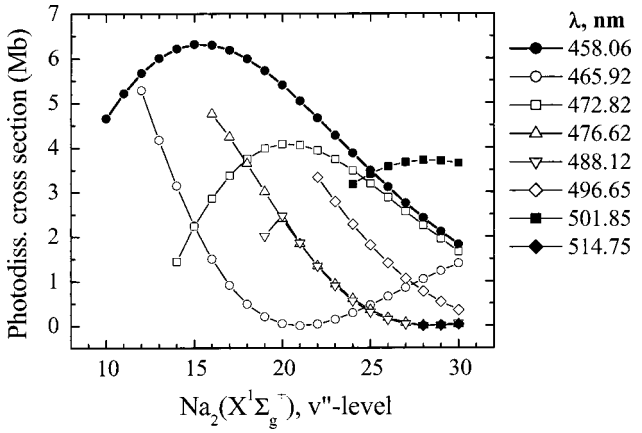


FIG. 6. Cross sections for the photodissociation of $Na_2$ ($X\,^1\Sigma_g^+,v'',J''=9$) molecules by 458 nm photons via the $B\,^1\Pi_u$ state as a function of the vibrational quantum number $v''$. For levels $v''\leqslant 9$ the energy $\varepsilon=E(v''J'')+h\nu_{Ar^+}$ is not sufficient to overcome the potential barrier of the $B\,^1\Pi_u$ state, the maximum of which lies 46 meV above the $3p_{3/2}+3s_{1/2}$ dissociation asymptote (Ref. 20). According to the calculations, for the initial level $v''=9$, $j''=9$ a narrow resonance is expected at about the energy of the 458 nm photon. However, in the experiment no detectable photofragment signals were observed at this wavelength when molecules were prepared to the level $v''=9$, $j''=9$. For comparison, photodissociation cross sections by other visible $Ar^+$ laser lines are also shown.

and

$$R_{X\,^1\Sigma_g^+,v''J''\rightarrow B\,^1\Pi_u,\varepsilon J'}=\int\chi_{X\,^1\Sigma_g^+,v''J''}(R)\mu(R)\chi_{B\,^1\Pi_u,\varepsilon J'}(R)dR. \quad (2)$$

The transition dipole moment curves $\mu(R)=e\langle X\,^1\Sigma_g^+|\Sigma q_i|B\,^1\Pi_u\rangle_{\rm el}$ (where $e$ is the electron charge and $q_i$ are the electronic coordinates) and the potential curves were taken from Ref. 26. The radial wave functions $\chi_{X\,^1\Sigma_g^+,v''J''}(R)$ and $\chi_{B\,^1\Pi_u,\varepsilon J'}(R)$ in Eq. (2) were integrated numerically using the Numerov method.[31] The resulting photodissociation cross sections for the range of vibrational levels of interest are given in Fig. 6. In the calculations we also checked for a possible contribution of the fragmentation of molecules into $Na(3p_{1/2})$ and $Na(3s_{1/2})$ atoms via the $A\,^1\Sigma_u^+$ state. We found that for the 458 nm photons this fragmentation channel is less efficient than the fragmentation via the $B\,^1\Pi_u$ state by several orders of magnitude and can thus be neglected. Besides the $A\,^1\Sigma_u^+$ and $B\,^1\Pi_u$ states there are no other singlet ungerade states in the accessible energy range, so that the $B\,^1\Pi_u$ state provides the only dissociation path.

### B. Photofragment angular distribution

With the given photodissociation cross sections and laser intensities, only a small fraction (less than 1%) of the molecules in the $(v_f'',J_f''=9)$ level are fragmented as they travel through the photodissociating laser beam. Therefore the rate of the photodissociation varies linearly with the intensity of the photodissociating laser, and the photofragment angular distribution does not depend on the laser intensity. As first shown by Zare and Hershbach,[32] the angular distribution of fragments ejected in a photodissociation process is generally anisotropic. The particular distribution depends on factors like the geometry of the experiment, polarization of the pho-

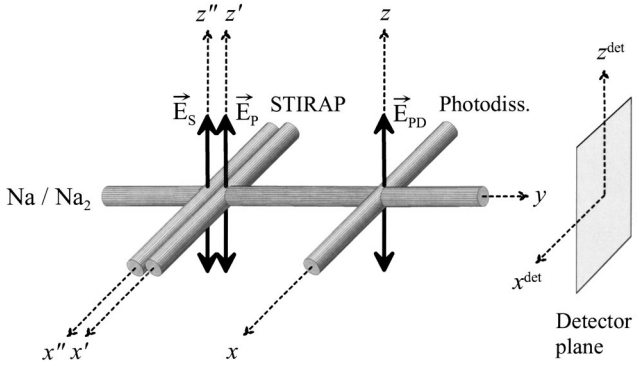


FIG. 7. Geometry of the photodissociation experiment. The molecular beam propagates along the $y$ axis toward the imaging detector. The Stokes and pump laser beams inducing population transfer by STIRAP, and the photodissociating laser beam cross the molecular beam at right angles, so that the axis $x''$, $x'$, and $x$ are all parallel. The light polarization vectors $\vec{E}_S$, $\vec{E}_P$, and $\vec{E}_{PD}$ of all three laser fields defining the direction of $z''$, $z'$, and $z$, respectively, are parallel to each other. The detector $x^{det}$-$z^{det}$ plane is parallel to the $x$-$z$ plane defined by the photodissociating laser.

todissociating laser beam, orientation of the dipole moment of the molecule, alignment or orientation of the molecules prior to dissociation, and the dynamics of the fragmentation process (see, e.g., Refs. 33–36 and references therein). We therefore performed calculations of the photofragment angular distribution for the given geometry of the experiment (see Fig. 7). Before the photodissociation, the molecules are transferred from the initial rovibronic level of the ground electronic state to the excited rovibronic level of the same electronic state by means of STIRAP. The transfer is induced by a $\Lambda$-scheme coupling involving the transitions $X\,^1\Sigma_g^+(v_i''=0,J_i''=9)\rightarrow A\,^1\Sigma_u^+(v',J'=10)\rightarrow X\,^1\Sigma_g^+(v_f'',J_f''=9)$. The Stokes and pump lasers are linearly polarized and their electric field vectors are parallel to each other (this direction defines the quantization axis). Since the optical selection rule $\Delta M=0$ applies here, the population transfer between the magnetic sublevels occurs in a set of pure three-level systems. Each set involves only the magnetic sublevels with the same magnetic quantum number $M$: $(J_i''=9,M)\rightarrow(J'=10,M)\rightarrow(J_f''=9,M)$. Hence, there are $2J_f''+1$ independent subsystems. The efficiency of population transfer is close to unity in each of them.

When the rotational levels are chosen such that $J_i''=J_f''<J'$, the number of magnetic sublevels in the intermediate $J'$ level is higher than in both lower levels. Therefore, the initial population distribution over $M$ will be mapped from $J_i''$ into $J_f''$. Thus, if the process starts from a rovibronic level with isotropically populated magnetic sublevels, the distribution in the final level will also be isotropic. Similarly, when $J_i''>J'>J_f''$, the final distribution will also be isotropic, though the population in sublevels with $|M|=J_i'',J_i''-1$ will remain in the initial state. When $J_i''=J_f''>J'$, the $|M|=J_f''$ sublevels in the final $J_f''$ level will remain unpopulated and thus the molecules will be aligned. For $J_f''>J'>J_i''$ a more pronounced alignment will be induced, since the levels $|M|=J_f'',J_f''-1$ remain unpopulated.

However, elastic and inelastic collision processes during the supersonic expansion lead to flow-induced alignment (see Ref. 37 for references on this subject). This occurs because the interaction potential between the scattering partners is anisotropic. The spatial distribution of angular momenta $n_J(\theta)$ around angle $\theta$ between the **J** vectors and the molecular beam axis is sensitive to the details of the expansion, like the pressure and temperature of the beam source, diameter, and shape of the nozzle. It can generally be described by an expansion of Legendre polynomials $n_J(\theta)=n_0\Sigma a_l P_l(\cos\theta)$, whereby only even-order polynomials occur because of cylindrical symmetry. From the existing studies of flow-induced alignment in $Na_2$ molecular beams[38–40] we conclude that under our experimental conditions the initial alignment is characterized by the value of the $a_2$ coefficient between $-0.1$ and $-0.4$, while the coefficients $a_4$ and higher are negligibly small. For $J_i''$, $J_f''<J'$, and $J_i''=J_f''$ the flow-induced alignment will be transferred by STIRAP to the final level $J_f''$.

The photodissociation thus starts from the aligned rovibronic level $v_f''$, $J_f''=9$ in the $X\,^1\Sigma_g^+$ state. The time of dissociation in a direct photodissociation is usually much shorter than the rotational period of the molecule. Therefore the fragments depart in the direction of the molecular axis at the moment of photodissociation. Since the direction of the transition dipole moment **d** is fixed to the molecular axis **r**, the photofragment angular distribution will reflect the distribution of **r** created by the polarized dissociating radiation field. Thus, the angular distribution of photofragments $f(\theta,\varphi)$ consists of two factors—the angular distribution of absorbing dipoles, $\rho(\theta,\varphi)$, and the absorption probability for each dipole, $G(\theta,\varphi)$. The latter is simply the Hermitian product of the transition dipole moment vector **d** and the light polarization vector **E**: $G(\theta,\varphi)=\mathbf{d}\cdot\mathbf{E}^*$. The angle $\theta$ is measured with respect to the quantization axis given by **E**.

When the projection $\Lambda$ of the electronic momentum of the diatomic molecule onto the internuclear axis does not change, as in transitions $\Sigma\rightarrow\Sigma$, $\Pi\rightarrow\Pi$, etc., the transition dipole moment of the optical transition is parallel to the molecular axis (the so-called parallel transitions).[36] The fragments will then preferentially recoil in the direction of the light polarization **E**. When the projection $\Lambda$ changes by $\Delta\Lambda=\pm1$ ($\Sigma\rightarrow\Pi$, $\Pi\rightarrow\Delta$, etc.) the transition dipole moment is perpendicular to the molecular axis (perpendicular transitions). Consequently, the recoil direction of the fragments will be complementary to the distribution of dipole moments immediately after the absorption. For isotropic distribution of the molecular axis (and, hence, the angular momenta) the well-known formula describing the photofragment angular distribution applies:[41]

$$f(\theta)\propto\frac{1}{4\pi}[1+\beta P_2(\cos\theta)], \tag{3}$$

where angle $\theta$ is measured with respect to the direction of laser polarization, and $\beta=2$ for a parallel and $\beta=-1$ for a perpendicular transition. The corresponding angular distribution of $X\,^1\Sigma_g^+\rightarrow B\,^1\Pi_u$ photodissociation fragments for the case when the photodissociating laser is polarized parallel and perpendicularly to the particle beam axis is shown in Figs. 8(a)–8(b). The angular distribution is affected by the flow-induced alignment. Figures 8(c)–8(d) show the photo-

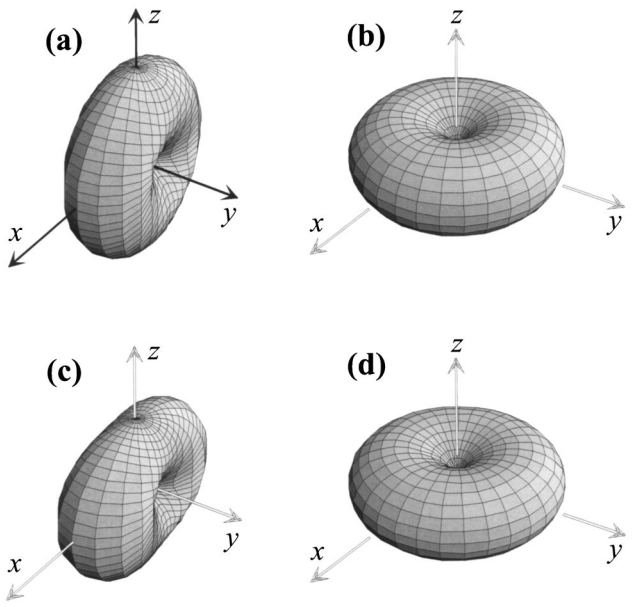


FIG. 8. Angular distribution of photofragments resulting from the photodissociation of $Na_2(X\ ^1\Sigma_g^+, v''J'')$ molecule via the $B\ ^1\Pi_u$ state. The choice of *x*, *y*, *z* axis is shown in Fig. 7. (a) and (b) are the isotropic distribution of the molecular axis prior to the dissociation with the photodissociation (PD) laser polarized parallel or perpendicular to the particle beam axis, respectively; (c) and (d) flow-induced alignment with $a_2 = -0.4$ and PD laser polarized parallel or perpendicular to the particle beam axis, respectively.

fragment distributions for the strongest possible flow-induced alignment with parameter $a_2 = -0.4$.

There are several ways to compare the experimental images with the theoretical 3-D distributions of the fragments. The most universal approach is to use the iterative forward convolution of the theoretical 3-D distribution over the experimental parameters to simulate the 2-D images.[44,45] Figure 9 shows an example of such forward convolution for the dissociation from level $v'' = 23$. For the convolution, 3-D photofragment distributions of Figs. 8(b) and 8(d) corresponding to the isotropic distribution of angular momenta prior to dissociation and flow-induced alignment with $a_2 = -0.4$ were used. A fraction of particles with zero energy perpendicular to the particle beam axis [the slow Na($3p$) atoms] are added to this Monte Carlo simulation, while the

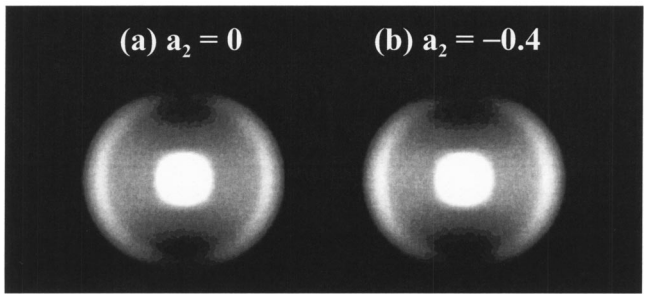


FIG. 9. The forward convolution of theoretical photofragment distributions of Figs. 8(b) and 8(d) for the photodissociation of molecules in rovibronic level $v'' = 23$, $J'' = 9$. The convolution takes into account the presence of a fraction of 0.2 of slow Na($3p$) atoms and the energy resolution of 50 meV. (a) The isotropic distribution of the molecular axis prior to dissociation; (b) flow-induced alignment with $a_2 = -0.4$.

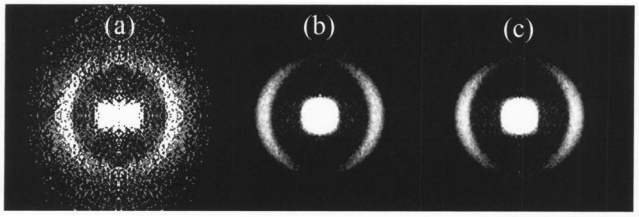


FIG. 10. Slices through the reconstructed 3-D recoil distributions of Na($3p_{3/2}$) fragments excited to high Rydberg states resulting from the photodissociation of $Na_2$ molecules selectively excited to the rovibronic level $v'' = 23$, $J'' = 9$. They were obtained by inverse Abel transformation of images shown in Figs. 5(b), 9(a), and 9(b). (a) Transformation of the experimental image [Fig. 5(b)]; (b) transformation of the simulated image with isotropic distribution of the molecular axis prior to dissociation [Fig. 9(a)]; (c) transformation of the simulated image with flow-induced alignment, $a_2 = -0.4$ [Fig. 9(b)].

convolution takes into account the 50 meV energy resolution of the experiment. A comparison with Fig. 5 confirms that such convolution reproduces the experimental 2-D images fairly well.

From Fig. 8 it is obvious that a laser polarization perpendicular to the particle beam axis, as realized in this experiment, is favorable for the data analysis, since the 3-D angular distribution of the fragments has cylindrical symmetry with the symmetry axis parallel to the 2-D detector plane. In such a situation the original 3-D distribution of the fragments can be reconstructed from the measured 2-D images using the inverse Abel transformation.[42,43] Figure 10(a) shows such a transformation of the experimental image of Fig. 5(b) for $v'' = 23$. Rotation of the reconstructed image around the symmetry axis yields the original 3-D distribution of the fragments. Figures 10(b)–10(c) show the inverse transformation of the simulated images in Fig. 9 for the dissociation of isotropically distributed and flow-aligned molecules. The photofragment angular dependence shown in Fig. 11 is obtained by suppressing the image due to slow Na($3p$) atoms and summing radially the ion counts for each angle $\theta$. The relatively small difference between the theoretical curves for the dissociation of molecules with an isotropically distributed axis and with flow-induced alignment with $a_2 = -0.4$ shows that the latter introduces only minor changes in the photofragment angular distribution. Although the scatter of experimental points does not allow us to draw quantitative conclusions about the flow-induced alignment, the simulated curve with $a_2 = -0.4$ is seen to be in somewhat better agreement with the experiment than the curve for an isotropic distribution.

Having reconstructed the original 3-D distribution of the atoms, we can now more accurately determine the ratio of the number of ''slow'' Na($3p$) atoms to the number of fast Na($3p$) photofragments. The transformed image in Fig. 10(a) represents the distribution of excited atoms in a section through the middle of a symmetric 3-D distribution, whereby the complete 3-D distribution is obtained by rotating the transformed image around the symmetry axis. Therefore before the determination of the ratio, each pixel of the transformed 2-D image must be weighted with $r = \rho \sin\theta$, where $r$ is the distance between the pixel and the symmetry axis, $\rho$ is the distance between the pixel and the center of the image,

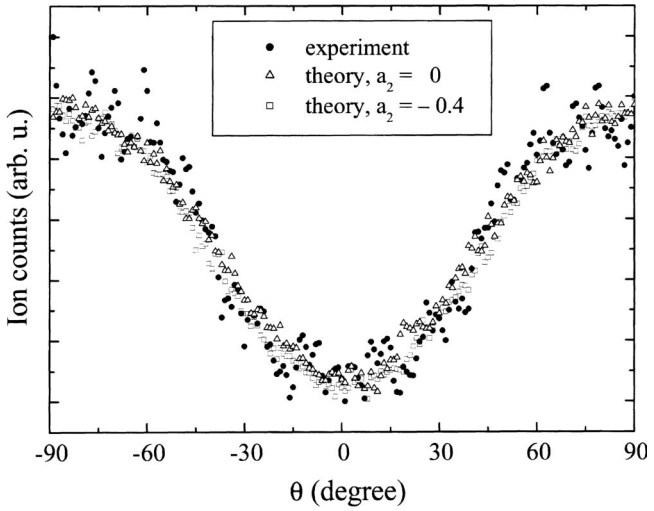


FIG. 11. Photofragment angular dependence for $v''=23$, as obtained from the reconstructed experimental and theoretical recoil distributions in Figs. 10(a)–10(c). It is obtained by summing radially the photofragment counts for each angle $\theta$. In the summation, the counts corresponding to the distribution of slow Na($3p$) atoms in the center each of the images in Figs. 10(a)–10(c) are suppressed. ●—experiment; △—isotropic distribution of molecular axis prior to dissociation; □—flow-induced alignment with $a_2=-0.4$.

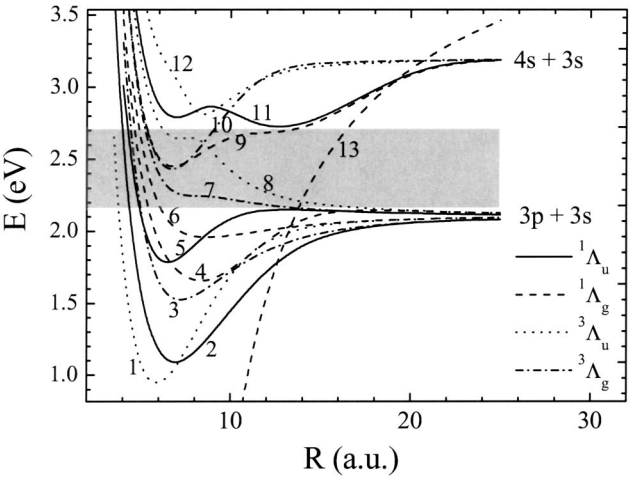


FIG. 12. Excited electronic states of $Na_2$ (Ref. 26): (1) $b\ ^3\Pi_u$; (2) $A\ ^1\Sigma_u^+$; (3) $1\ ^3\Sigma_g^+$; (4) $2\ ^1\Sigma_g^+$; (5) $B\ ^1\Pi_u$; (6) $1\ ^1\Pi_g$; (7) $1\ ^3\Pi_g$; (8) $3\ ^3\Sigma_u^+$; (9) $3\ ^1\Sigma_g^+$; (10) $2\ ^3\Sigma_g^+$; (11) $2\ ^1\Sigma_u^+$, (12) $3\ ^3\Sigma_u^+$, (13) $^1\Sigma_g^+$ ($Na^+ + Na^-$). The greyed area marks the energies that are reached from vibrational levels $10 \leqslant v'' \leqslant 23$ in the ground electronic state by photons from either the $Ar^+$ laser or the frequency doubled ps laser.

and $\theta$ is the angle relative to the symmetry axis.[7] After such weighting, we obtain that the ratio of numbers of slow and fast excited atoms, $N_{Na^*_{slow}}/N_{Na^*_{fast}}$, is 0.16 and 0.22 for the photodissociation from levels $v''=17$ and $v''=23$, respectively.

## V. ANALYSIS: EFFICIENT FORMATION OF SLOW Na($3p$) BY RADIATIVE EXCITATION TRANSFER

In the discussion below we shall refer to Na($3p$) atoms as *fast* when their velocity differs significantly from that of the flow velocity of the particle beam, and *slow* when their velocity is about equal with the flow velocity. For the observation of slow Na($3p$) atoms besides the fast fragments resulting from the photodissociation process (1) rises the question about the mechanism that is responsible for their formation. A production of slow Na($3p$) fragments in a two-photon dissociation process of $Na_2$ can be excluded. Only the 458 nm radiation from the $Ar^+$ laser and the frequency doubled radiation ($\lambda \approx 408$ nm) from the ps mode-locked laser are available for such a process in the reaction region. The absorption of two $Ar^+$ laser photons would either ionize the vibrationally excited $Na_2$ molecules creating a bound $Na_2^+$ ion or excite them to a Rydberg state. The latter is expected to autoionize and should be detectable as $Na_2^+$ ions. No ions were detected in the experiment when the ps laser was shut off. Absorption of one $Ar^+$ laser photon and one frequency doubled photon (the same is valid also for the absorption of two frequency doubled photons) can energetically lead to the photodissociation of vibrationally excited $Na_2$ into an $Na^+$ ion and a Na($3s$) atom. However, such a process does not explain the change in the image of slow particles upon tuning the frequency doubled laser photons to below the $Na(3p)+h\nu \rightarrow Na^+ + e$ ionization threshold.

Three other mechanisms could, in principle, lead to the formation of Na($3p$) atoms with small momentum relative to the flow velocity of the primary beam: (a) energy transfer (ET) from electronically excited $Na_2$ molecules to slow Na($3s$) atoms in the primary beam; (b) resonant ET from fast Na($3p$) photofragments to slow Na($3s$) atoms from the beam; (c) radiative excitation transfer from fast Na($3p$) to slow Na($3s$) from the beam via the phenomenon of radiation trapping. We consider each of these mechanisms separately.

### A. Energy transfer from excited $Na_2$ molecules

Energy transfer from excited $Na_2$ molecules is the most straightforward mechanism. The slow Na($3p$) atoms are produced by collisional energy transfer from an electronically excited molecule to the Na($3s$) atoms in the primary beam:

$$Na_2^*(^1\Lambda_u) + Na(3s) \rightarrow Na_2(X\ ^1\Sigma_g^+) + Na^*(3p).$$

The studies of this process involving bound rovibronic levels of the $A\ ^1\Sigma_u^+$ and $B\ ^1\Pi_u$ states of $Na_2$[46–48] have shown that the corresponding cross sections are usually of an order of $10^{-14}$ cm$^2$. In particularly favorable cases, when the energy change in the molecule approximately matches that in the atom, the cross sections are as large as $10^{-13}$–$10^{-12}$ cm$^2$.[49–51] Nevertheless, this mechanism has to be ruled out because there are no bound states of $^1\Sigma_u^+$ or $^1\Pi_u$ symmetry, which could be excited from the vibrationally excited levels $v'' \geqslant 10$ in the ground $X\ ^1\Sigma_g^+$ state by either the $Ar^+$ laser or the frequency doubled ps laser radiation (see Fig. 12). Excitation from the level $v''=0$, in which the molecules are initially concentrated after the supersonic expansion, can also be excluded. The 458 nm $Ar^+$ laser line could excite the molecules to bound rovibronic levels of the $A\ ^1\Sigma_u^+$ or the $B\ ^1\Pi_u$ state, while the frequency doubled laser radiation around 408 nm would dissociate the molecules into the $Na(3s)+Na(3p)$ fragments if only the photon energies are

considered. However, the Franck–Condon factors for that excitation scheme are negligibly small. Accordingly, no Na($3p$) atoms (and no ions) were observed in the experiment when the STIRAP lasers were switched off, showing that only vibrationally excited molecules lead to the formation of excited atoms.

### B. Resonant ET from fast Na($3p$) to slow Na($3s$)

Collisional excitation transfer from the fast Na($3p_{3/2}$) photofragments to the slow Na($3s$) atoms of the primary beam,

$$\text{fast Na}^*(3p_{3/2}) + \text{slow Na}(3s_{1/2}) \rightarrow \text{fast Na}(3s_{1/2}) + \text{slow Na}^*(3p_{3/2}), \quad (4)$$

is possible. The experimental studies (see the review;[52] Ref. 53 gives more recent references) have shown that the collisional energy transfer between fine structure components $j=1/2$ and $j=3/2$ of resonance states proceeds in alkali typically with cross sections of an order of $10^{-14}$ cm$^2$. The process (4) is, however, a resonant process. Therefore its cross section can be expected to be even larger. For this reason we only consider the process (4) and disregard the complementary process in which slow atoms in the other $j$-component, $3p_{1/2}$, are produced.

The resonant process (4) is very efficient because of the dipole–dipole interaction between the atoms:

$$V(R) = \frac{\mathbf{D}_1\mathbf{D}_2 - 3(\mathbf{D}_1\mathbf{n})(\mathbf{D}_2\mathbf{n})}{R^3},$$

where $\mathbf{D}_1$ and $\mathbf{D}_2$ are the dipole operators of the colliding atoms, $\mathbf{n}$ is the unit vector of the direction between the atoms (internuclear axis), and $R$ is the internuclear distance. Estimates of the cross section given in Ref. 54 lead to a simple dependence on the reduced dipole matrix element $D$ of the resonance transition and the collision velocity $v$ (in atomic units):

$$\sigma \sim D^2/v.$$

For $D \sim 1$ and room temperature velocities the cross section is very large, $\sigma \sim 1/v \sim (10^{-13}-10^{-12})$ cm$^2$. The energy transfer in (4) occurs mainly at large impact parameters and, hence, small scattering angles. Therefore the momentum transfer between the colliding partners is small and the slow Na($3p_{3/2}$) atoms do not depart from the vicinity of the particle beam axis.

A more detailed quantitative analysis[55,56] shows that for the $^2P_{3/2} \rightarrow {}^2S_{1/2}$ transitions the average cross section can be expressed as

$$\sigma(^2P_{3/2}, {}^2S_{1/2}) = 1.66\frac{\pi S}{v}, \quad (5)$$

where $S$ is connected with the strength of the $3p_{3/2} \rightarrow 3s_{1/2}$ transition and is thus related to the radiative lifetime $\tau$ of the $3p_{3/2}$ level,

$$S = \frac{3}{64\pi^3}\frac{\lambda^3}{\tau}. \quad (6)$$

Substituting $\tau = 16.25$ ns, $\lambda_{\text{vac}} = 589.16$ nm, and $v = 913$ m/s [for a representative kinetic energy of 0.1 eV that the fast Na($3p$) fragments acquire in the dissociation] in (5) and (6), one obtains $\sigma = 1.1 \times 10^{-12}$ cm$^2$.

Knowing the cross section of the process (4), one can estimate the ratio of the slow and fast Na($3p$) atoms. Assuming that the slow Na($3p$) atoms are produced by process (4) and decay by spontaneous emission, this process can be described by a rate equation,

$$\frac{dn^*_{\text{slow}}}{dt} = \sigma v\, n_0 n^*_{\text{fast}} - \frac{n^*_{\text{slow}}}{\tau}, \quad (7)$$

where $n_0$, $n^*_{\text{slow}}$, and $n^*_{\text{fast}}$ are the number densities of Na($3s_{1/2}$), slow Na($3p_{3/2}$), and fast Na($3p_{3/2}$) atoms, respectively. The pulse-to-period ratio of the ionizing ps laser is of the order of $10^{-4}$, so that the ionization rate of Na($3p$) atoms can be disregarded in the balance equations. Furthermore, both the time necessary for the fast Na($3p$) photofragments to leave the particle beam and the time the atoms need for travel through the photodissociating laser beam are much larger than the lifetime of the $3p$ state. One can therefore assume steady-state conditions for the process (7). The ratio of the number densities of slow to fast Na($3p$) atoms, which is equal with the measured ratio of numbers of slow and fast excited atoms, thus becomes

$$\frac{n^*_{\text{slow}}}{n_{\text{fast}}} = \sigma v\, \tau n_0 = 3.3 \times 10^{-4}. \quad (8)$$

This ratio is by nearly three orders of magnitude smaller than the experimentally measured ratio, hence the process (4) can explain the formation of only a small fraction of the observed slow Na($3p$) atoms.

### C. Formation of slow Na($3p$) atoms by radiative excitation transfer from fast Na($3p$) photofragments

So far we have neglected a process that often affects experiments involving atoms in the resonance states, namely, radiation trapping on atomic resonance transitions that was first described by Milne,[57] Holstein,[58] and Biberman[59] in the first half of the last century. If an excited atom is surrounded by other atoms of the same species in the ground state at high enough densities, the resonance radiation will be absorbed and reemitted many time before it escapes from the volume occupied by the atoms. These multiple reabsorptions and reemission of photons will thus decrease the effective radiative decay rate of the sample compared to the natural radiative decay rate $\Gamma_{\text{nat}}$:

$$\Gamma_{\text{eff}} = g\Gamma_{\text{nat}}, \quad (9)$$

where $g$ is a dimensionless escape factor that can be regarded as the reciprocal of the number of emission and absorption events before the escape.

Radiation trapping has two important consequences in the context of the present experiment. First, it implies that the spontaneous lifetime $\tau = 1/\Gamma_{\text{nat}}$ in Eq. (8) has to be replaced by an effective lifetime $\tau_{\text{eff}} = 1/\Gamma_{\text{eff}}$ increased due to the radiation trapping. This, in turn, will lead to an increase in the ratio (8). The calculations performed in a future

paper[16] (hereafter referred to as Paper II) show that under the conditions of the opacity $\kappa_0 R = 0.37$ and beam radius $R = 1$ mm used in the present experiment, the escape factor $g = 0.42$, so that $\tau_{\text{eff}} = 2.35\tau$. With this value the ratio (8) becomes $7.8\times10^{-4}$. This value is still much smaller than the ratios of 0.16 and 0.22 measured in the experiment. Therefore, even with radiation trapping properly taken into account, the resonant ET process (4) gives only a minor contribution to the formation of slow Na($3p$) atoms.

Another consequence of radiation trapping is the absorption of photons that are emitted by the fast Na($3p_{3/2}$) photofragments by the abundant Na($3s_{1/2}$) atoms from the primary beam, leading to the formation of slow Na($3p_{3/2}$) atoms. In Ref. 60 it was shown that radiation trapping plays a dominant role in the thermalization of velocity selected excited atoms in thermal vapors. Such a mechanism is feasible also under the conditions of the present experiment because the spontaneous lifetime of the $3p_{3/2}$ state is much shorter than the average time the photofragments need to escape from the primary particle beam. Most of the excited photofragments are therefore expected to emit a photon while surrounded by the Na($3s$) atoms at a density of $2\times10^{11}$ cm$^{-3}$.

The detailed derivation of the theory of velocity redistribution of excited atoms by radiation trapping is given in Paper II. Here we shall provide only a brief outline of this theory and describe its consequences for the present experiment. In the collimated supersonic beam employed in the present experiment, the $1/e$ width of velocity distribution of Na($3s$) atoms along the beam axis measures $\Delta v_{\parallel} = 300$ m/s. In the direction perpendicular to the beam axis the atoms are collimated to a divergence of 0.8°, which yields a velocity spread of $\Delta v_{\perp} = 9$ m/s. Such a small transverse velocity spread allows us to assume for further mathematical analysis that the beam is ideally collimated, i.e., we neglect the deviations of the velocity vectors of atoms from the direction of the particle beam axis $\vec{e}_y$. The normalized velocity distribution $f(\vec{v})$ of Na($3s$) atoms in the beam thus becomes

$$f(\vec{v}) = \delta(v_x)\,\delta(v_z) f_b(v_y);$$
$$f_b(v) = \frac{1}{\sqrt{\pi}\Delta v_{\text{at}}} \exp\left(-\frac{v^2}{\Delta v_{\text{at}}^2}\right); \quad \int_{-\infty}^{\infty} dv\, f_b(v) = 1. \tag{10}$$

The velocity $v_y$ is measured relative to the beam flow velocity $v_f = 1340$ m/s. The value $\Delta v_{\text{at}} = \Delta v_{\parallel} = 300$ m/s gives the width of the distribution function $f_b(v)$. Furthermore, we assume that the spectral absorption and emission profiles, $\kappa_\nu$ and $\varphi_\nu$, are determined by the Doppler width. The absorption coefficient for a photon of frequency $\nu$ moving in the direction $\vec{n}$ is then given by the relation[61]

$$\kappa_\nu = \overline{\sigma}^{(r)} \Gamma_{\text{nat}} n_0 \frac{c}{\nu_0} \int d^3v\, f(\vec{v})\, \delta\left(\vec{n}\vec{v} - \frac{\nu-\nu_0}{\nu_0} c\right);$$
$$\overline{\sigma}^{(r)} = \frac{\lambda^2}{8\pi}\frac{g_2}{g_1}, \tag{11}$$

where $c$ is the speed of light, $\nu_0$ and $\lambda$ are the frequency and wavelength of resonance photons in the center of the line, and $g_1 = 2$ and $g_2 = 4$ are the statistical weights of the lower $3s_{1/2}$ and the upper $3p_{3/2}$ levels, respectively. Using the distribution (10), Eq. (11) can be reduced to the form

$$\kappa_\nu = \frac{\kappa_0}{|\cos\theta|}\sqrt{\pi}\Delta v_{\text{at}} f_b\left(\frac{\tilde{v}}{|\cos\theta|}\right); \quad \tilde{v} = \frac{\nu-\nu_0}{\nu_0} c;$$
$$\kappa_0 = \frac{\lambda^3}{8\pi^{3/2}}\frac{g_2}{g_1}\frac{\Gamma_{\text{nat}}}{\Delta v_{\text{at}}} n_0. \tag{12}$$

Here, $\theta$ is the angle between the $y$ (i.e., beam) axis and the direction $\vec{n}$ of photon propagation, and $\kappa_0 = 3.7$ cm$^{-1}$ is the absorption coefficient at the line center at $\lambda = 589.16$ nm. From Eq. (12) it is clear that the absorption at the line center is large in the directions perpendicular to the particle beam axis because the Doppler linewidth decreases with angle $\theta$, $\Delta\nu_{\text{D}} \sim |\cos\theta|$. This effect outweighs the relatively small opacity $\kappa_0 R = 0.37$ at beam radius $R = 1$ mm, so that radiation imprisonment becomes noticeable under the conditions of a well-collimated supersonic beam.

Quantitatively the effect of radiation trapping is described by the generalized Holstein–Biberman equation[58,59,62] determining the evolution of the excited state density $n^*$ as a function of space coordinate $\vec{r}$:

$$\frac{\partial n^*(\vec{r}, v_y, t)}{\partial t}$$
$$= -\Gamma_{\text{nat}} n^*(\vec{r}, v_y, t) + \Gamma_{\text{nat}} \int_{v_y'} \int_{\Omega} d^3r'$$
$$\times dv_y'\, n^*(\vec{r}', v_y', t) G(\vec{r}, \vec{r}', v_y, v_y')$$
$$+ S(\vec{r}, v_y, t). \tag{13}$$

Here, $G(\vec{r}, \vec{r}', v_y, v_y')$ gives the probability that radiation emitted at point $\vec{r}'$ will be absorbed at point $\vec{r}$, and $S(\vec{r}, v_y, t)$ is the source term (cm$^{-3}$ s$^{-1}$) describing the external excitation rate, which in the present context corresponds to excitation of Na($3s_{1/2}$) atoms by photons emitted by fast Na($3p_{3/2}$) photofragments. Such a separation of the source term is justified because the number density of fast Na($3s_{3/2}$) photofragments is smaller (by several orders of magnitude) than the density of slow Na($3s_{3/2}$) atoms in the beam. Therefore the reverse process, in which the fast Na($3s_{1/2}$) atoms [which either arise from fast Na($3p_{3/2}$) after they have emitted a photon, or represent the other dissociation fragment] absorb the photons emitted by slow Na($3p_{3/2}$), is negligibly inefficient. In other words, the fast Na atoms seed the excitation into the system of slow atoms and leave the beam, while the system of slow atoms diffuses this excitation within the beam. In addition, the emission/absorption profiles of fast atoms are much broader than those of slow atoms, which further reduces the probability of diffusing the excitation back from the slow to the fast atoms.

In such a situation, the same considerations as those given above after the rate equation (7) apply, and it is reasonable to treat Eq. (13) under steady-state conditions:

$$\Gamma_{\text{nat}} n^*_{\text{slow}}(\vec{r}, v_y) = S(\vec{r}, v_y) + \Gamma_{\text{nat}} \int_{v_y'} \int_{\Omega_b} d^3r'\, dv_y'$$
$$\times n^*_{\text{slow}}(\vec{r}', v_y) G(\vec{r}, \vec{r}', v_y, v_y'), \tag{14}$$

where $\Omega_b$ is the beam volume and $S(\vec{r},v_y)$ is determined by the interplay of the emission profile of excited photofragments and the absorption profile of atoms in the primary beam. The integral on the right-hand side of Eq. (14) describes the radiation imprisonment in the system of slow Na atoms from the primary beam. In the case of an ideally collimated beam the functions entering Eq. (14) can be factorized in parts depending on the spatial variables and the velocity $v_y$. The Doppler effect implies that for the atom emitting a photon and for the atom absorbing this photon the conservation of the velocity projection onto the photon emission direction $\vec{n}$ should fulfill $(v_y^{(1)}\vec{e}_y)\vec{n}=(v_y^{(2)}\vec{e}_y)\vec{n}$, i.e., $v_y^{(1)}=v_y^{(2)}$. In other words, the velocity component $v_y$ of slow atoms involved in the emission-reabsorption process does not change. Furthermore, advantage can be taken of the possibility to factorize the source function. Since the emission profile $\varepsilon_\nu$ of fast photofragments is much broader than the absorption profile $\kappa_\nu$, one can assume that $\varepsilon_\nu \cong \varepsilon_{\nu=0} \cong$const within the absorption width. Therefore at the limit of small opacities the intensity $I_\nu(\vec{r})$ of radiation emitted by fast photofragments is nearly the same for all absorption frequencies of the slow Na($3s_{1/2}$) atoms at any point $\vec{r}$ inside the beam: $I_\nu(\vec{r})\sim\varepsilon_\nu\cong\varepsilon_{\nu=0}\cong$const. The source function can then be expressed as

$$S(\vec{r},v_y)=\kappa_{\tilde{\nu}}I_{\tilde{\nu}}(\vec{r})\sim f_b(v_y)\varepsilon_{\tilde{\nu}}\cong f_b(v_y)\varepsilon_{\nu=0}\cong\text{const}\times f_b(v_y),$$

where $\tilde{\nu}$ is the Doppler shifted frequency seen by the absorbing atoms, $\tilde{\nu}=\nu_0+v_y/\lambda\cdot\cos\theta$. The above equation implies that the velocity profile of the source function, which can be written as $S(\vec{r},v_y)/S(\vec{r},v_y=0)=f_b(v_y)/f_b(v_y=0)$, does not depend on the spatial coordinate $\vec{r}$. This is true for vanishingly small opacities. At non-negligible opacities the absorption of photons inside the beam lead to a deformation of the intensity profile $I_\nu(\vec{r})$, and the ratio $S(\vec{r},v_y)/S(\vec{r},v_y=0)$ begins to deviate from the initial velocity distribution $f_b(v_y)/f_b(v_y=0)$ of slow atoms in the beam. As it is shown in Paper II, this deviation is very small at the opacities of the present experiment. Therefore we can affirm with a sufficient accuracy that the source function can be factorized as $S(\vec{r},v_y)=S(\vec{r})f_b(v_y)$, where $S(\vec{r})\equiv S(\vec{r},v_y=0)/f_b(v_y=0)$.

The above considerations allow us to substitute in Eq. (14) $n^*_{\text{slow}}(\vec{r},v_y)=n^*_v(\vec{r})f_b(v_y)$ and to consider Eq. (14) for each subensemble of atoms with fixed velocity $v_y=v$ separately:

$$n^*_v(\vec{r})-\int_{\Omega_b}d^3r'\,n^*_v(\vec{r}')G_v(\vec{r},\vec{r}')=\frac{S(\vec{r})}{\Gamma_{\text{nat}}};$$
$$G_v(\vec{r},\vec{r}')=\frac{1}{4\pi|\vec{r}-\vec{r}'|^2}\kappa_v\exp(-\kappa_v|\vec{r}-\vec{r}'|), \tag{15}$$

where $\kappa_v=(\kappa_0/|\cos\theta|)\exp[-v^2/(\Delta v_{\text{at}}^2\cos^2\theta)]$ and $\theta$ is the angle between the beam axis and the direction of the vector $\vec{r}-\vec{r}'$. Since the kernel $G_v(\vec{r},\vec{r}')$ is an exponentially decreasing function of its spatial variables, Eq. (15) can be evaluated using the Fokker–Planck method. The calculations in Paper II show that the number of slow Na($3p$) atoms can be expressed by a simple relation:

TABLE I. Experimental and theoretical ratios of the numbers of slow and fast Na($3p$) atoms formed after the photofragmentation of $Na_2$ in the levels $v''=17$ and $v''=23$.

| $Na_2$ $v''$ level | $N_{Na^*_{slow}}/N_{Na^*_{fast}}$ | | |
|---|---|---|---|
| | Experiment | Theory, without HFS | Theory, with HFS |
| 17 | 0.16 | 0.26 | 0.13 |
| 23 | 0.22 | 0.21 | 0.19 |

$$N_{\text{Na}^*_{\text{slow}}}=\Omega_{\text{PD}}S(\vec{r}=0)\frac{1}{g\Gamma_{\text{nat}}}, \tag{16}$$

where $\Omega_{\text{PD}}$ is the volume of the photodissociation zone, and the source function $S(\vec{r}=0)$ in the center of $\Omega_{\text{PD}}$ is determined by the density $n^*_{\text{fast}}$ and velocity $v_{\text{PD}}$ of the excited photofragments,

$$S(\vec{r}=0)=\Gamma_{\text{nat}}n^*_{\text{fast}}\kappa_0R\frac{15\pi\sqrt{\pi}}{64}\frac{\Delta v_{\text{at}}}{v_{\text{PD}}}\left(1+\frac{1}{8}\frac{\Delta v_{\text{at}}^2+\Delta v_{\text{mol}}^2}{v_{\text{PD}}^2}+\frac{\sqrt{2}}{\pi}\kappa_0R[\ln(\kappa_0R)-1.17]\right). \tag{17}$$

Substituting Eq. (17) into Eq. (16), the ratio of numbers of slow and fast Na($3p$) atoms is expressed as

$$\frac{N_{\text{Na}^*_{\text{slow}}}}{N_{\text{Na}^*_{\text{fast}}}}=\frac{15\pi^{3/2}}{64}\frac{\kappa_0R}{g}\frac{\Delta v_{\text{at}}}{v_{\text{PD}}}\left(1+\frac{1}{8}\frac{\Delta v_{\text{at}}^2+\Delta v_{\text{mol}}^2}{v_{\text{PD}}^2}+\frac{\sqrt{2}}{\pi}\kappa_0R[\ln(\kappa_0R)-1.17]\right), \tag{18}$$

where $N_{\text{Na}^*_{\text{fast}}}=n^*_{\text{fast}}\Omega_{\text{PD}}$. Inserting the respective values of photofragment velocities $v_{\text{PD}}=857$ m/s and $v_{\text{PD}}=1065$ m/s, we obtain for the ratio (18) the values of 0.26 and 0.21 for the photodissociation from the levels $v''=17$ and $v''=23$, respectively. Interestingly, the main contribution to the population of the slow Na($3p$) atoms is due to the photons emitted by photofragments perpendicularly to their fragmentation velocity regardless of the direction of the fragmentation. Although these theoretical values are in a fairly good agreement, the measured ones (see Table I), they show a tendency reversed to that observed in the experiment: the theoretical ratio is larger for the dissociation from the lower vibrational level, whereas the experimental ratio is larger for the dissociation from the higher vibrational level.

This disagreement can be abolished by taking into account the hyperfine splitting of Na energy levels. As shown in the thermalization study of excited atoms,[60] a non-negligible hyperfine splitting should be taken into account when considering the radiation imprisonment. The hyperfine splitting in the excited $3p_{3/2}$ state into $F=0$, 1, 2, and 3 sublevels is not resolved because it is much smaller than the Doppler width $\Delta\nu_{\text{D}}=\Delta v_{\text{at}}/\lambda=500$ MHz associated with the velocity distribution $f_b(v)$ of Na($3s$) atoms in the beam. In contrast, the 1772 MHz splitting between the $F=1$ and $F=2$ sublevels of the $3s_{1/2}$ state is considerably larger than $\Delta\nu_{\text{D}}$. In Paper II it is shown that under such conditions the radiation diffusion is described as two independent imprison-

ment processes occurring on the hyperfine transitions $3p_{3/2} \rightarrow 3s_{1/2}$, $F=1$ and $3p_{3/2} \rightarrow 3s_{1/2}$, $F=2$. It leads to a decreased effective opacity of the medium $\kappa_0^{(\mathrm{eff})}R \approx \sqrt{15}/8\kappa_0 R = 0.19$ and an increased effective escape factor $g_{\mathrm{eff}}=0.56$. For the level $v''=17$, the width of the emission profile of fast $\mathrm{Na}(3p_{3/2})$ photofragments, which is determined by the Doppler shift due to fragmentation velocity, extends $\Delta\nu = \pm 1453$ MHz from the center of each hyperfine transition and does not reach the frequency of the other hyperfine transition. The effective ratio of slow to fast $\mathrm{Na}(3p)$ atoms is therefore expressed as a sum of two contributions corresponding to two hyperfine transitions:

$$\left.\frac{N_{\mathrm{Na}^*_{\mathrm{slow}}}}{n_{\mathrm{Na}^*_{\mathrm{fast}}}}\right|_{\mathrm{eff}} = \left.\frac{N_{\mathrm{Na}^*_{\mathrm{slow}}}}{N_{\mathrm{Na}^*_{\mathrm{fast}}}}\right|_{F=1} + \left.\frac{N_{\mathrm{Na}^*_{slow}}}{N_{\mathrm{Na}^*_{\mathrm{fast}}}}\right|_{F=2}, \tag{19}$$

where

$$\left.\frac{N_{\mathrm{Na}^*_{\mathrm{slow}}}}{N_{\mathrm{Na}^*_{\mathrm{fast}}}}\right|_{F} = \frac{15\pi^{3/2}}{64}\frac{\overline{g}_F\kappa_0^{(F)}R}{8g_{\mathrm{eff}}}\frac{\Delta v_{\mathrm{at}}}{v_{\mathrm{PD}}}\left(1+\frac{1}{8}\frac{\Delta v_{\mathrm{at}}^2+\Delta v_{\mathrm{mol}}^2}{v_{\mathrm{PD}}^2} + \frac{\sqrt{2}}{\pi}\kappa_0^{(F)}R[\ln(\kappa_0^{(F)}R)-1.17]\right).$$

Here, $\overline{g}_F = 2F+1$ is the statistical weight of the hyperfine level $F$ of the ground state $3s_{1/2}$, the total weight of the $3s_{1/2}$ state is $3+5=8$, and $\kappa_0^{(F)} = \kappa_0\overline{g}_F/8$ is the respective partial absorption coefficient of the hyperfine transition. Equation (19) yields a ratio of 0.13 for $v''=17$.

In the case of dissociation from the level $v''=23$, the fragmentation velocity $v_{\mathrm{PD}}=1065$ m/s is large enough to increase the width of the photofragment emission profile to $\Delta\nu = \pm 1805$ MHz. Under such conditions, the photons emitted by photofragments on each of the hyperfine transitions can be absorbed by both hyperfine levels $F=1$ and $F=2$ simultaneously, and the ratio of slow to fast $\mathrm{Na}(3p)$ atoms is given by the relation

$$\left.\frac{N_{\mathrm{Na}^*_{\mathrm{slow}}}}{N_{\mathrm{Na}^*_{\mathrm{fast}}}}\right|_{\mathrm{eff}} = \frac{15\pi^{3/2}}{64}\frac{\kappa_0 R}{g_{\mathrm{eff}}}\frac{\Delta v_{\mathrm{at}}}{v_{\mathrm{PD}}}\left(1+\frac{1}{8}\frac{\Delta v_{\mathrm{at}}^2+\Delta v_{\mathrm{mol}}^2}{v_{\mathrm{PD}}^2} + \frac{\sqrt{2}}{\pi}\kappa_0^{(\mathrm{eff})}R[\ln(\kappa_0^{(\mathrm{eff})}R)-1.17]\right). \tag{20}$$

From Eq. (20) we obtain for $v''=23$ a ratio of 0.19, which is larger than that for $v''=17$. One can see from Table I that the mechanism of radiative excitation transfer, which accounts for the HFS of the $3s_{1/2}$ state, correctly reproduces the experimental observations. Note, that the larger ratio for $v''=23$ is explained solely by the different conditions under which the source function is formed. For $v''=17$, the radiation emitted by the fast photofragments on a given hyperfine transition is absorbed on the corresponding hyperfine transition of slow Na atoms, whereas for $v''=23$ the absorption takes place on both hyperfine transitions of the slow atoms simultaneously.

## VI. CONCLUSION

In this paper we have presented a detailed study of the photodissociation process $\mathrm{Na}_2(X\,^1\Sigma_g^+, v'', J'') + h\nu_{458\,\mathrm{nm}} \rightarrow \mathrm{Na}_2^*(B\,^1\Pi_u) \rightarrow \mathrm{Na}^*(3p) + \mathrm{Na}(3s)$ in a supersonic beam. We use laser manipulation to prepare the molecules prior to dissociation selectively in predetermined quantum states. A novel design of ion imaging apparatus with a permanently field-free reaction zone was used to obtain two-dimensional images of photofragments. Fragments with kinetic energies differing by 50 meV could be resolved. The photofragment angular distributions provided by two-dimensional images reflect the flow-induced alignment of molecules in the beam prior to dissociation, though its effect is not dramatic.

An important observation made in this study is the efficient formation of excited $\mathrm{Na}(3p)$ atoms that have not acquired momentum relative to the flow velocity. Such atoms cannot result from direct dissociation. The use of the imaging technique allowed us to separate the fast $\mathrm{Na}(3p_{3/2})$ atoms produced in the direct photodissociation process from slow $\mathrm{Na}(3p_{3/2})$ atoms produced in a secondary process. It was identified as the excitation of $\mathrm{Na}(3s)$ atoms from the primary beam to the $3p_{3/2}$ state by photons emitted by the fast $\mathrm{Na}(3p_{3/2})$ photofragments. This process could be well described in terms of the radiation trapping phenomenon. The solution of the radiation trapping equation allowed us to express the ratio of slow excited atoms created in a secondary process to the fast photodissociation fragments by simple analytical formulas. A very good agreement with the experimental observations is obtained, when the non-negligible hyperfine splitting of the Na ground state is taken into account. In this study we thus demonstrate that radiation trapping can imply dramatic changes in the apparent translation energy distribution of excited species after a unimolecular fragmentation process. Note that the radiative excitation transfer is on one hand similar to the dipole–dipole resonance excitation transfer discussed in Sec. V B, in the sense that the latter process can be seen as an exchange of virtual photons between the fast and the slow atoms. On the other hand it is different, since the former process is an exchange of real photons between atoms. For the resonance excitation transfer to take place, a sufficiently close encounter of atoms is necessary. Therefore this process is efficient only at sufficiently high atom densities, which are seldom achieved in beam experiments. In the process of radiation imprisonment, in contrast, the excitation is transferred by photons and close encounters of atoms are not necessary. In principle, for the imprisonment only the opacity is of importance, and it can be efficient also at low densities provided that the extension of the media is sufficiently large. In conclusion, we emphasize the importance of a proper account of radiation trapping phenomenon in any experiment involving atoms in resonance states, even in media-like supersonic beams, where one intuitively expects the effect of radiation trapping to be negligible.

## ACKNOWLEDGMENTS

This work was supported by the Deutsche Forschungsgemeinschaft. One of the authors (A.E.) was supported by

the EU Marie Curie Individual Fellowship HPMF-CT-1999-00080. Partial support by the INTAS-2001-155 grant, the Latvian Science Council, and the NATO Collaboration Linkage, Grant No. PST.CLG. 979120, are acknowledged. We thank H. Hotop for helpful discussions.

[1] W. R. Simpson, A. J. Orr-Ewing, and R. N. Zare, Chem. Phys. Lett. **212**, 163 (1993).
[2] M. Brouard, S. Duxon, P. A. Enriquez, and J. P. Simons, J. Chem. Soc., Faraday Trans. **89**, 1435 (1993).
[3] J. W. Hepburn, in *Atomic and Molecular Beam Methods*, edited by G. Scoles (Oxford University Press, New York, 1992), Vol. 2, p. 261.
[4] T. Oster, A. Kühn, and E. Illenberger, Int. J. Mass Spectrom. Ion Processes **89**, 1 (1989).
[5] D. W. Chandler and P. L. Houston, J. Chem. Phys. **87**, 1445 (1987).
[6] P. L. Houston, J. Phys. Chem. **100**, 12757 (1996).
[7] A. J. R. Heck and D. W. Chandler, Annu. Rev. Phys. Chem. **46**, 335 (1995).
[8] D. H. Parker, in *Photoionization and Photodetachment, Part 1*, Advanced Series in Physical Chemistry, Vol. 10A, edited by C.-Y. Ng (World Scientific, Singapore, 2000), p. 3.
[9] D. W. Chandler and D. H. Parker, in *Advances in Photochemistry, Vol. 25*, edited by D. C. Neckers, D. H. Volman, and G. von Bünau (Wiley, New York, 1999), p. 59.
[10] B. J. Whitaker, in *Research in Chemical Kinetics, Vol. 1*, edited by R. G. Compton and G. Hancock (Elsevier, Amsterdam, 1993), p. 307.
[11] T. F. Gallagher, *Rydberg Atoms* (Cambridge University Press, Cambridge, 1994).
[12] A. Ekers, O. Kaumann, and K. Bergmann, Latv. J. Phys. Tech. Sci. **1**, 51 (2002).
[13] O. Kaufmann, A. Ekers, C. Gebauer-Rochholz, K. U. Mettendorf, M. Keil, and K. Bergmann, Int. J. Mass. Spectrom. **205**, 233 (2001).
[14] O. Kaufmann, A. Ekers, C. Gebauer-Rochholz, and K. Bergmann, in preparation for Rev. Sci. Instrum.
[15] K. Bergmann, H. Theuer, and B. W. Shore, Rev. Mod. Phys. **70**, 1003 (1998); U. Gaubatz, P. Rudecki, S. Schiemann, and K. Bergmann, J. Chem. Phys. **92**, 5363 (1990).
[16] N. N. Bezuglov, A. Ekers, O. Kaufmann, K. Bergmann, F. Fuso, and M. Allegrini, J. Chem. Phys. (submitted).
[17] N. Yonekura, C. Gebauer, H. Kohguchi, and T. Suzuki, Rev. Sci. Instrum. **70**, 3265 (1999).
[18] M. Szilagyi, *Electron and Ion Optics* (Plenum, New York, 1988).
[19] A. T. J. B. Eppink and D. H. Parker, Rev. Sci. Instrum. **68**, 3477 (1997); D. H. Parker and A. T. J. B. Eppink, J. Chem. Phys. **107**, 2357 (1997).
[20] E. Tiemann, Z. Phys. D: At., Mol. Clusters **5**, 77 (1987).
[21] M. L. Janson and S. M. Papernov, J. Phys. B **15**, 4175 (1982).
[22] G. Gerber and R. Möller, *AIP Conference Proceedings*, Vol. 146, edited by R. G. Lerner (American Institute of Physics, Woodbury, NY, 1986).
[23] E. W. Rothe, U. Krause, and R. Düren, J. Chem. Phys. **72**, 5145 (1980); Chem. Phys. Lett. **72**, 100 (1980).
[24] G. Gerber and R. Möller, Phys. Rev. Lett. **55**, 814 (1985).
[25] E. A. Gordeev, E. E. Nikitin, and A. I. Sushin, Mol. Phys. **33**, 1611 (1977).
[26] I. Schmidt, *Dissertation* (Universität Kaiserslautern, Kaiserslautern 1987). The potentials and transition moment functions are available upon request from W. Meyer.
[27] J.-A. Beswick and J. Durup, in *Half Collisions Induced by Lasers*, Proceedings of the Summer School on Chemical Physics, Les Houches, France, edited by P. Glorieux, D. Lecler, and R. Vetter (CNRS, Paris, 1979).
[28] A. Messiah, *Quantum Mechanics* (North-Holland, Amsterdam, 1962), Vol. 2.
[29] I. Kovacs, *Rotational Structure in the Spectra of Diatomic Molecules* (Adam Hilger, London, 1969).
[30] B. R. Judd, *Angular Momentum Theory for Diatomic Molecules* (Academic, New York, 1975).
[31] B. R. Johnson, J. Chem. Phys. **67**, 4086 (1977).
[32] R. N. Zare and D. R. Hershbach, Proc. IEEE **51**, 173 (1963).
[33] R. Schinke, *Photodissociation Dynamics* (Cambridge University Press, New York, 1993).
[34] R. N. Zare, Mol. Photochem. **4**, 1 (1972).
[35] R. N. Zare, *Angular Momentum* (Wiley, New York, 1988).
[36] M. Auzinsh and R. Ferber, *Optical Polarization of Molecules* (Cambridge University Press, New York, 1995).
[37] V. Aquilanti, D. Ascenzi, M. de Castro Vitores, F. Pirani, and D. Cappelletti, J. Chem. Phys. **111**, 2620 (1999).
[38] M. P. Sinha, C. D. Caldwell, and R. N. Zare, J. Chem. Phys. **61**, 491 (1974).
[39] A. G. Visser, J. P. Bekooy, L. K. van der Meij, C. de Vreugd, and J. Korving, Chem. Phys. **20**, 391 (1977).
[40] U. Hefter, G. Ziegler, A. Mattheus, A. Fischer, and K. Bergmann, J. Chem. Phys. **85**, 286 (1986).
[41] R. J. van Brunt and R. N. Zare, J. Chem. Phys. **48**, 4304 (1968).
[42] R. N. Strickland and D. W. Chandler, Appl. Opt. **30**, 1811 (1991).
[43] L. M. Smith and D. R. Keefer, J. Quant. Spectrosc. Radiat. Transf. **39**, 367 (1988).
[44] L. S. Bontuyan, A. G. Suits, P. L. Houston, and B. J. Whitaker, J. Phys. Chem. **97**, 6342 (1993).
[45] A. S. Bracker, E. R. Wouters, A. G. Suits, and O. S. Vasyutinskii, J. Chem. Phys. **110**, 6749 (1999).
[46] M. L. Janson and J. P. Klavins, Chem. Phys. Lett. **86**, 453 (1982); E. K. Kraulinya, E. K. Kopeikina, and M. L. Janson, *ibid.* **39**, 565 (1976).
[47] E. K. Kraulinya and M. L. Yanson, Opt. Spectrosc. **46**, 629 (1979); E. K. Kopeikina and M. L. Yanson, *ibid.* **41**, 217 (1976).
[48] H. Hulsman and P. Willems, Chem. Phys. **119**, 377 (1988).
[49] M. Jansons, J. Klavins, V. Grushevsky, L. Caiyan, and S. Svanberg, Z. Phys. D: At., Mol. Clusters **31**, 55 (1994).
[50] G. Baumgartner, H. P. Keller, and W. Preuss, Z. Phys. D: At., Mol. Clusters **1**, 295 (1986).
[51] J. Derouard and N. Sadeghi, Chem. Phys. Lett. **111**, 353 (1984).
[52] L. Krause, Adv. Chem. Phys. **28**, 267 (1975).
[53] C. Vadla, M. Movre, and V. Horvatic, J. Phys. B **27**, 4611 (1994); M. Movre, V. Horvatic, and C. Vadla, *ibid.* **32**, 4647 (1999); V. Horvatic, C. Vadla, M. Movre, and K. Niemax, Z. Phys. D: At., Mol. Clusters **36**, 101 (1996).
[54] B. M. Smirnov, *Excited Atoms* (Energoatomizdat, Moscow, 1982) (in Russian).
[55] T. Watanabe, Phys. Rev. **138**, A1573 (1965); Adv. Chem. Ser. **82**, 176 (1968).
[56] Yu. A. Vdovin and N. A. Dobrodeev, Sov. Phys. JETP **28**, 544 (1969).
[57] E. Milne, J. London Math. Soc. **1**, 1 (1926).
[58] T. Holstein, Phys. Rev. **72**, 1212 (1947).
[59] L. M. Biberman, Zh. Eksp. Teor. Fiz. **17**, 416 (1947).
[60] J. Huennekens, R. K. Namiotka, J. Sagle, Z. J. Jabbour, and M. Allegrini, Phys. Rev. A **51**, 4472 (1995).
[61] V. V. Ivanov, *Transfer of Radiation in Spectral Lines*, NBS Special Publication No. 385 (U.S. GPO, Washington, 1973).
[62] T. Holstein, Phys. Rev. **83**, 1159 (1951).